

Multi-dimensional seismic response control of offshore platform structures with viscoelastic dampers (II-Experimental study)

Xiao-Yu He^{*1}, Tie-Wei Zhao², Hong-Nan Li³ and Jun Zhang⁴

¹Zhejiang Provincial Planning, Design & Research Institute of Communications, Hangzhou 310006, P.R. China

²Ningbo Port and Waterway Administration, Ningbo, 315041, P.R. China

³State Key Laboratory of Coastal and Offshore Engineering, Dalian University of Technology, Ganjingzi District, Linggong Road 2, Dalian, 116024, P.R. China

⁴State Grid Zhejiang Electric Power Company, Hangzhou, 310007, P.R. China

(Received December 31, 2015, Revised March 23, 2016, Accepted March 25, 2016)

Abstract. Based on the change of traditional viscoelastic damper structure, a brand-new damper is designed to control simultaneously the translational vibration and the rotational vibration for platforms. Experimental study has been carried out on the mechanical properties of viscoelastic material and on its multi-dimensional seismic response control effect of viscoelastic damper. Three types of viscoelastic dampers with different shapes of viscoelastic material are designed to test the influence of excited frequency, strain amplitude and ambient temperature on the mechanical property parameters such as circular dissipation per unit, equivalent stiffness, loss factor and storage shear modulus. Then, shaking table tests are done on a group of single-storey platform systems containing one symmetric platform and three asymmetric platforms with different eccentric forms. Experimental results show that the simulation precision of the restoring force model is rather good for the shear deformation of viscoelastic damper and is also satisfied for the torsion deformation and combined deformations of viscoelastic damper. The shaking table tests have verified that the new-type viscoelastic damper is capable of mitigating the multi-dimensional seismic response of offshore platform.

Keywords: viscoelastic damper; platform; multi-dimensional seismic response; seismic control

1. Introduction

During the past few years, extensive analytical and experimental studies have been carried out to investigate the performance of viscoelastic dampers (VED) as energy-dissipation devices for structural applications (Mahmoodi 1969, Lin *et al.* 1991, Chang *et al.* 1992, Bergman and Hanson 1993, Chang *et al.* 1995). Results from these studies showed that the response of structures to earthquakes can be reduced significantly due to notable increase in structural damping. The corresponding structural responses due to seismic loading also decreased accordingly. However, analytical and test results also showed that, although the damper can be effective in attenuating

*Corresponding author, Ph.D., E-mail: rainy0649@126.com

seismic response of the structure, the proper design for maximum efficiency must take into account important factors such as excitation frequency, structure natural frequency and working environment temperature.

A typical VED consists of thin layers of viscoelastic material and steel plates. So far researchers all over the world have developed multiform VEDs (Zhou 2006), such as bitumen rubber composition (BRC) VED, lath-type VED, arm-type VED, lever VED, distinguished themselves on constitution and viscoelastic material from the typical VED. The VED is also one of the most popular control devices for the seismic control research of offshore platforms. Lee (1997) used the VED to mitigate the vibration of an offshore structural system in the marine environment and verified that the VED has high energy absorption capacity. Ou *et al.* (Ou *et al.* 1999, Ou *et al.* 2000, Ou *et al.* 2002) analyzed the dynamic performances of platform structure with a set of viscoelastic energy dissipators. Ma *et al.* (Ma *et al.* 2004) studied the dynamic response of an actual multi-degree freedom offshore platform equipped with the VEDs and optimized the position of VED. The VED absorbs earthquake energy by transforming the shear deformation energy into heat. However, typical VEDs are usually installed in single frame side of structures connected by braces and work only in one horizontal direction. However, the new-type VED developed in this paper will be proposed due to its superiority of capacity for bi-directional shear deformation. It is known that the earthquake motion is essentially multi-dimensional and so is the corresponding structural response. Therefore, multi-component seismic response of offshore platform can be controlled by installing typical VEDs in both frame side directions and can also be well controlled by installing the proposed new-type VED in single deck plane.

This paper is concerned with the experimental study on the mechanical properties of viscoelastic material and the multi-dimensional seismic response control of the VED. Three types of VEDs with different shapes of viscoelastic material are designed and made in the test to examine the influence of the excitation frequency, strain amplitude and ambient temperature on the mechanical property parameters of circular dissipation per unit, equivalent stiffness, loss factor and storage shear modulus. Then the shaking table tests are carried on a group of single-storey platform systems containing one symmetric platform and three asymmetric platforms with different eccentric forms.

2. Working principle for the multi-dimensional control of viscoelastic dampers

The new-type VED used in this paper is different from the typical VED in both construction feature and installation form. Schematic diagrams for the construction and installation form are shown in Figs. 1 and 2, respectively. The essential difference between the two types of VEDs lies in the plane relationship between viscoelastic material and platform deck. When the deformation of platform deck occurs in all possible directions, bi-directional shear deformation will take place in the new-type VED with parallel position relationship between viscoelastic material and platform deck while unidirectional shear deformation will take place in the typical VED with perpendicular position relationship between viscoelastic material and platform deck. Due to its bi-directional deformation capacity, the new-type VED can consume more energy than the common typical VED. Hence the cost of seismic control can be reduced.

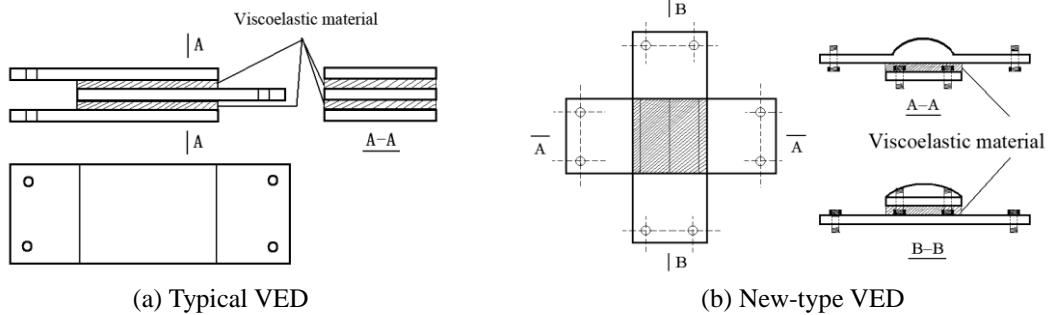


Fig. 1 Structure scheme for the viscoelastic dampers

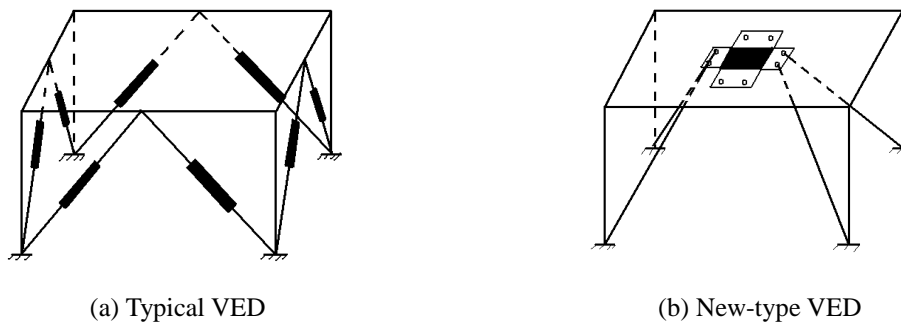


Fig. 2 Setting of different viscoelastic dampers

3. Mechanical property test on VED

3.1 Test setup and test program

The plane graphs of three VEDs with different shapes of viscoelastic material used in this test are shown in Fig. 3. Shear areas of viscoelastic material of the three VEDs, A , are designed to be identical with the parameters $r=35.7$ mm, $a=63.2$ mm, $b=40$ mm, $h=100$ mm. The upper and lower connecting steel planes are identically designed for the three VEDs with the upper plane dimension 220 mm \times 100 mm and the lower plane dimension 220 mm \times 160 mm. Fig. 4 gives the spatial graphic for the integral damper and its components.

The purpose of this experiment is to learn the mechanical property of the VED and then to establish the restore force model of the VED in order to make necessary preparations for the following shaking table test. The influence of excited loading frequency, strain amplitude, ambient temperature and cycling loading times on the characteristic parameters of VED is investigated through the pure shear deformation test. Then the torsion deformation capacity and the combined deformation capacity of shear and torsion are studied, respectively.

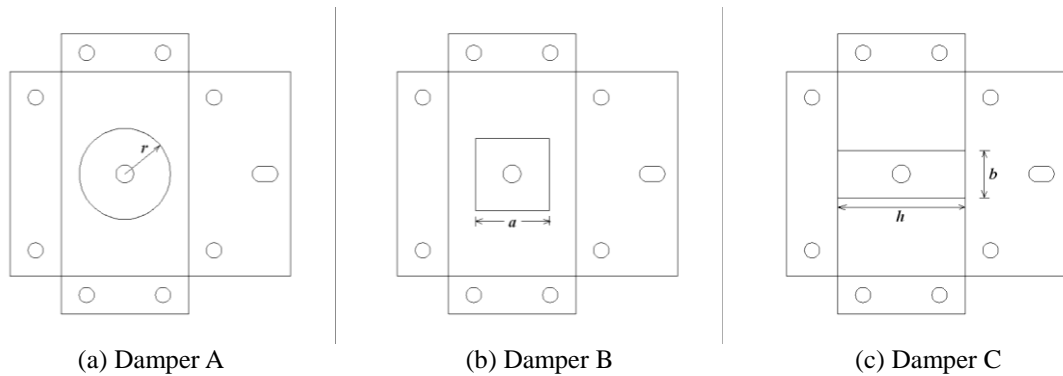


Fig. 3 Plane graph of three viscoelastic dampers

The ZN-I damping compound is chosen for the VED in test and this experiment is conducted in the state key laboratory of structural analysis for industrial equipment. The VED is connected by the localizing frame and the test machine of MTS810. Fig. 5 shows the experimental setup graphs for the shear and torsion deformation tests and the combined deformation test.

Total six excited loading frequencies (0.1 Hz, 0.5 Hz, 1.0 Hz, 2.0 Hz, 4.0 Hz and 8.0 Hz) are applied in the test, for considering the frequency range of practical engineering. Five strain amplitudes, λ_{max} , including 20%, 40%, 60%, 80% and 100% are considered by controlling the deflection of control point. The thickness of viscoelastic material, d , is 10 mm here, thus the deflection of control point should be 2 mm, 4 mm, 6 mm, 8 mm and 10 mm, respectively. The mechanical property test are conducted at three ambient temperatures of 18°C, 23°C and 28°C, respectively. The ambient temperature chosen here is restricted by the test condition. According to the property of viscoelastic material, the new-type VED designed in this paper can work for the ambient temperature changing from -20°C to 40°C.

The schematic force-displacement curve of viscoelastic damper is shown in Fig. 6, with the expression as follows

$$\left(\frac{f - k'u}{\eta k'u_0}\right)^2 + \left(\frac{u}{u_0}\right)^2 = 1 \tag{1}$$

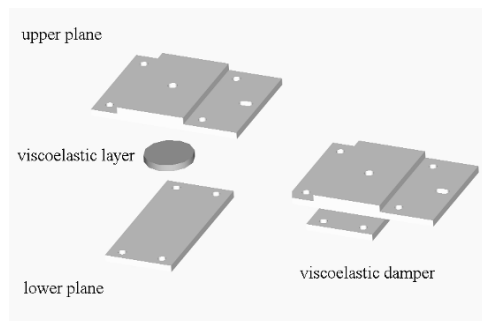


Fig. 4 Spatial graphic for integral damper and its components

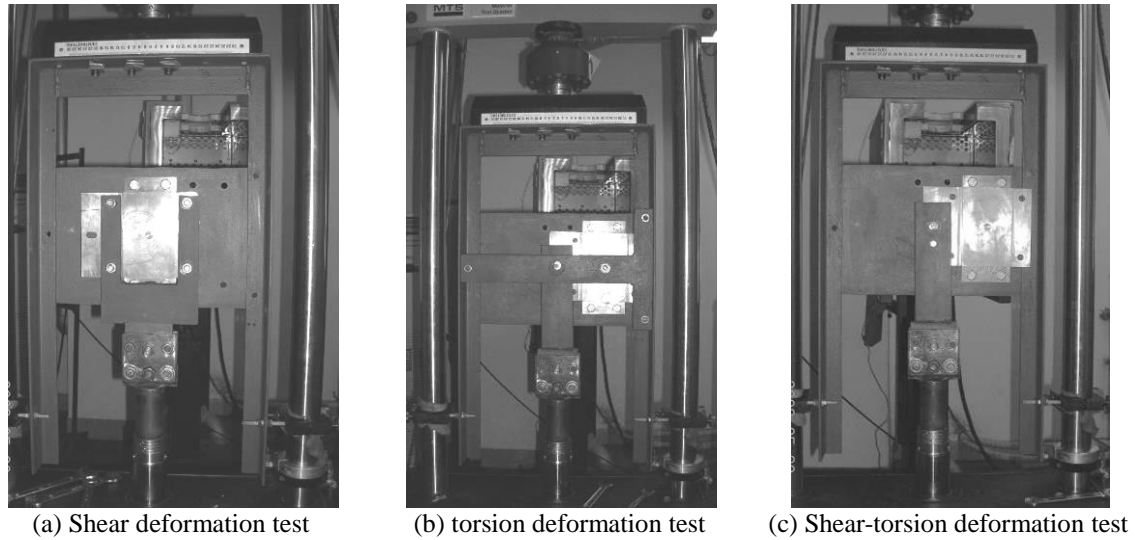


Fig. 5 Experimental setup

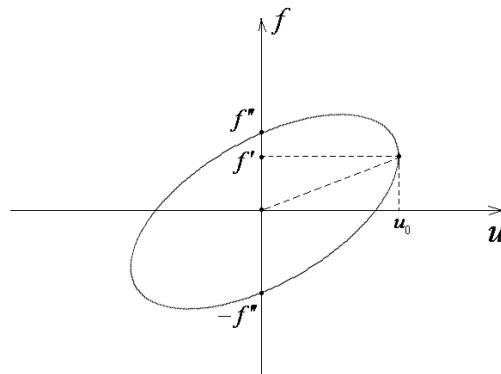


Fig. 6 Schematic force-displacement curve of viscoelastic damper

where u_0 is the maximum displacement and f' denotes the restoring force corresponding to u_0 . f'' means the restoring force when $u=0$ with the specific expression of $f''=\eta k'u_0$ and k' implies the equivalent stiffness of the VED with the expression of $k'=f'/u_0$. Four characteristic parameters are obtained for the comparison of the mechanical property of the VED: (1) circular dissipation per unit E_d , that is the area surrounded by the restoring force curve; (2) equivalent stiffness k' ; (3) loss factor η and (4) storage shear modulus G' ($G'=k'd/A$).

3.2 Results of test

3.2.1 Influence of excited frequency

In this section the test is conducted at the ambient temperature of 23°C and the strain amplitude

is controlled by 40%. The restoring force curves of the VED for damper A, damper B and damper C subjected to different frequency sinusoidal excitations are shown in Fig. 7. The relation curves of storage shear modulus and loss factor with different excitation frequencies are given in Fig. 8. Table 1 lists the results of the characteristic parameters obtained from different frequency tests. It is clear from the test data that the excitation frequency has a great influence on the characteristic parameters. When the strain amplitude of the VED keeps invariant, all the characteristic parameters E_d , k' , η and G' will increase with the increase of excitation frequency.

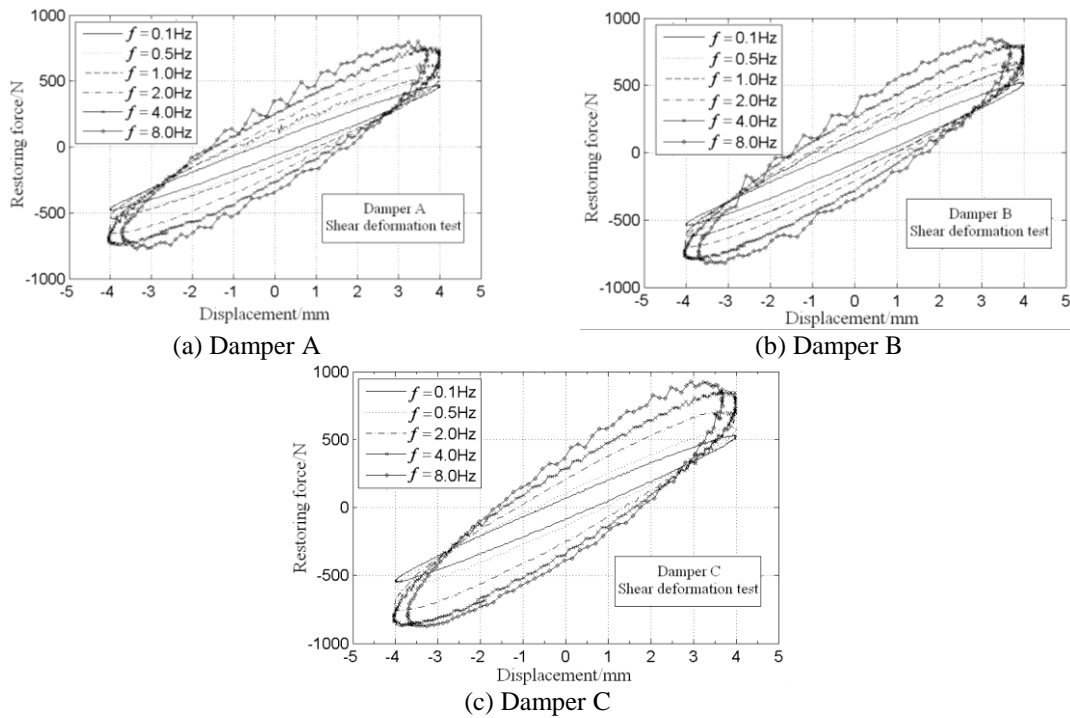


Fig. 7 Force-displacement curve of viscoelastic damper for different loading frequencies

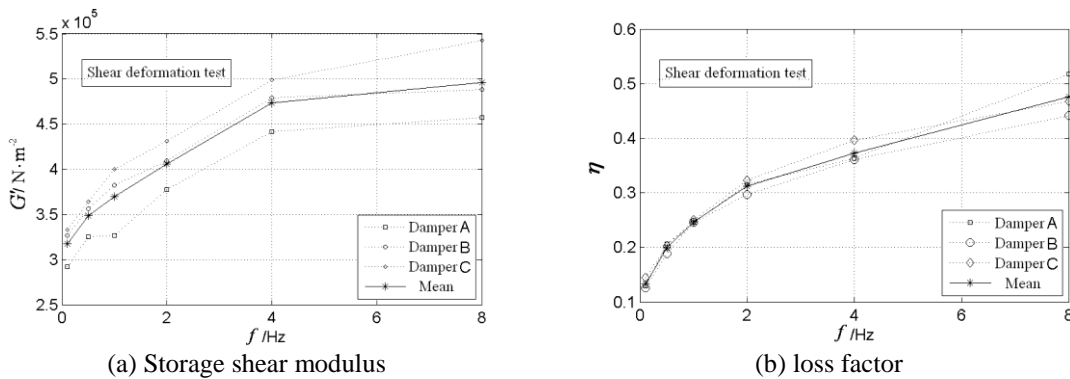


Fig. 8 Relationship between characteristic parameters and loading frequencies

Table 1 Characteristic parameters tested for different loading frequencies

f/Hz	$E_d/\text{N}\cdot\text{m}$			$k'/\text{N}\cdot\text{m}^{-1}$		
	Damper A	Damper B	Damper C	Damper A	Damper B	Damper C
0.1	0.7858	0.8751	0.9760	1.1697E+05	1.3056E+05	1.3323E+05
0.5	1.2618	1.3713	1.5180	1.3009E+05	1.4232E+05	1.4563E+05
1.0	1.6212	1.8443	--*	1.3080E+05	1.5267E+05	--*
2.0	2.4297	2.4865	2.9267	1.5115E+05	1.6339E+05	1.7245E+05
4.0	3.3375	3.4466	4.0451	1.7697E+05	1.9128E+05	1.9961E+05
8.0	3.9269	4.0589	4.6316	1.8314E+05	1.9502E+05	2.1707E+05
f/Hz	η			$G'/\text{N}\cdot\text{m}^{-2}$		
	Damper A	Damper B	Damper C	Damper A	Damper B	Damper C
0.1	0.1293	0.1256	0.1448	2.9213E+05	3.2687E+05	3.3307E+05
0.5	0.2067	0.1881	0.2031	3.2492E+05	3.5631E+05	3.6408E+05
1.0	0.2451	0.2460	--*	3.2668E+05	3.8223E+05	--*
2.0	0.3156	0.2965	0.3222	3.7750E+05	4.0906E+05	4.3113E+05
4.0	0.3625	0.3606	0.3961	4.4200E+05	4.7890E+05	4.9903E+05
8.0	0.5169	0.4418	0.4675	4.5740E+05	4.8825E+05	5.4268E+05

* --: missed measure test data

Table 2 Characteristic parameters tested for different strain amplitudes

$\lambda_{\max}/\%$	$E_d/\text{N}\cdot\text{m}$			$k'/\text{N}\cdot\text{m}^{-1}$		
	Damper A	Damper B	Damper C	Damper A	Damper B	Damper C
20	0.4469	0.4527	0.5175	1.4872E+05	1.5708E+05	1.6399E+05
40	1.6210	1.8366	--*	1.3080E+05	1.5394E+05	--*
60	3.6170	3.7531	4.1920	1.3225E+05	1.4367E+05	1.5060E+05
80	5.9920	6.3308	7.0473	1.2380E+05	1.3719E+05	1.4306E+05
100	8.0095	9.3043	10.3800	1.0777E+05	1.3140E+05	1.3494E+05
$\lambda_{\max}/\%$	η			$G'/\text{N}\cdot\text{m}^{-2}$		
	Damper A	Damper B	Damper C	Damper A	Damper B	Damper C
20	0.2520	0.2260	0.2478	3.7144E+05	3.9328E+05	4.0997E+05
40	0.2451	0.2394	--*	3.2668E+05	3.8541E+05	--*
60	0.2472	0.2252	0.2420	3.3030E+05	3.5970E+05	3.7649E+05
80	0.2377	0.2222	0.2360	3.0919E+05	3.4348E+05	3.5766E+05
100	0.2288	0.2157	0.2302	2.6915E+05	3.2897E+05	3.3736E+05

* --: missed measure test data

3.2.2 Influence of strain amplitude

In this section the test is conducted at the ambient temperature of 23°C and the excitation frequency is 1 Hz. Table 2 lists the results of the characteristic parameters obtained from different strain amplitude tests. The relation curves of storage shear modulus and loss factor with different strain amplitudes are given in Fig. 8. The restoring force curves of the VED for damper A, damper B and damper C with different strain amplitudes are shown in Fig. 9. It is clear from the test data that the circular dissipation per unit E_d will increase while other parameters k' , η and G' will decrease with the increase of strain amplitude.

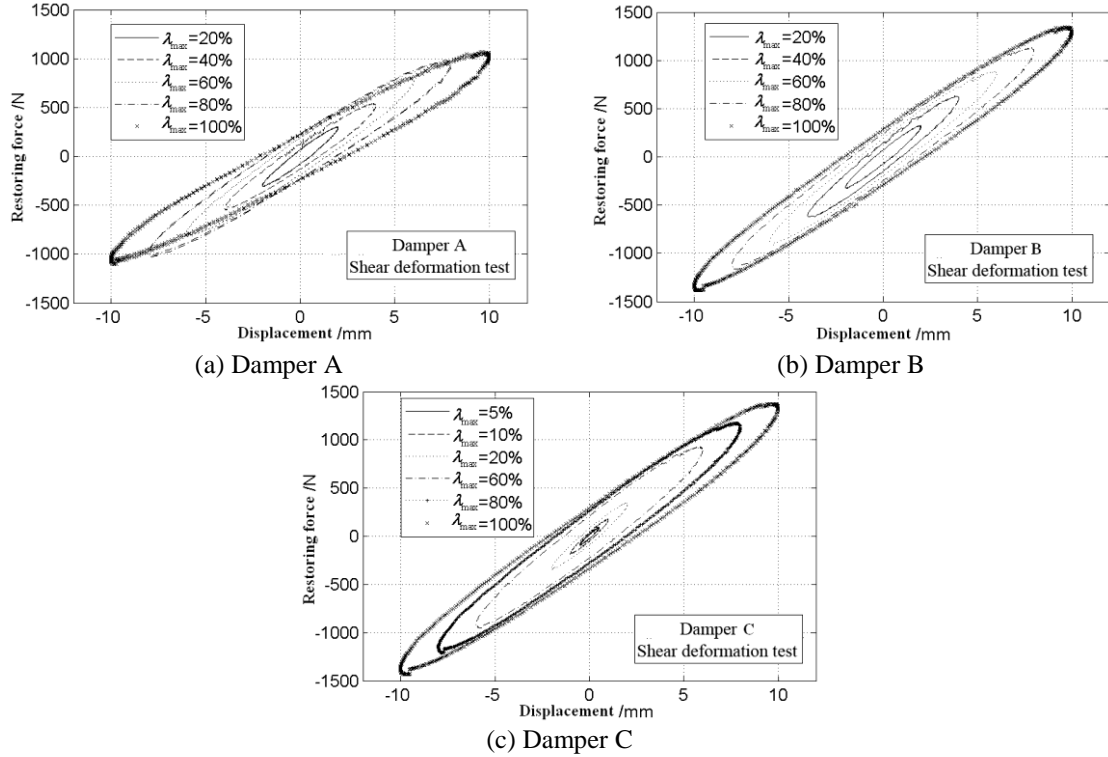


Fig. 9 Force-displacement curve of viscoelastic damper for different strain amplitude

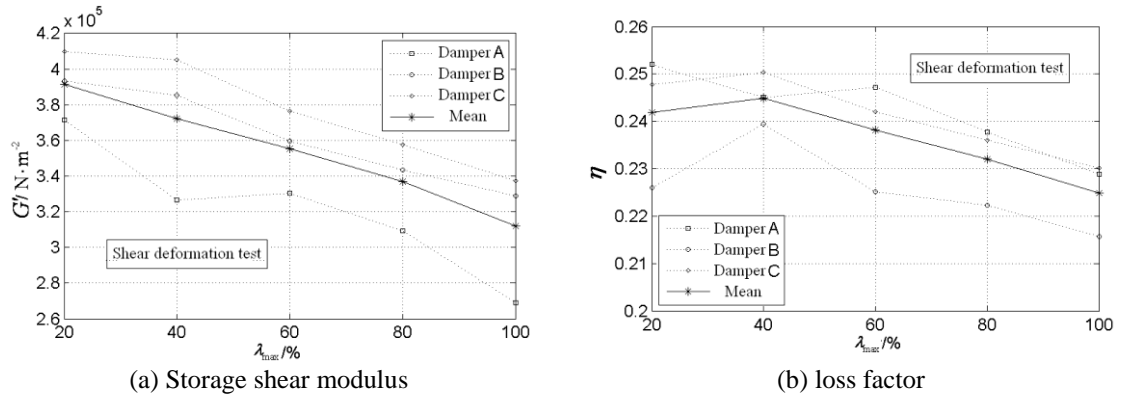


Fig. 10 Relationship between characteristic parameters and strain amplitude

3.2.3 Influence of ambient temperature

In this section the strain amplitude is controlled by 40% and the excitation frequency is 1Hz. The restoring force curves of the VED for damper A, damper B and damper C at different ambient temperatures are shown in Fig. 11. Table 3 lists the results of the characteristic parameters obtained from different strain amplitude tests. It is shown from the test data that the parameters E_d , k' , η and G' will decrease with the increase of ambient temperature from 18°C to 28°C.

Table 3 Characteristic parameters tested for different ambient temperatures

$T / ^\circ\text{C}$	$E_d / \text{N} \cdot \text{m}$			$k' / \text{N} \cdot \text{m}^{-1}$		
	Damper A	Damper B	Damper C	Damper A	Damper B	Damper C
18	1.8846	2.5579	2.7368	1.1387E+05	1.5723E+05	1.6296E+05
23	1.6376	1.8147	--*	1.1237E+05	1.4985E+05	--*
28	1.4945	1.4627	1.8532	1.0237E+05	1.3534E+05	1.4663E+05

$T / ^\circ\text{C}$	η			$G' / \text{N} \cdot \text{m}^{-2}$		
	Damper A	Damper B	Damper C	Damper A	Damper B	Damper C
18	0.3312	0.3275	0.3434	2.8440E+05	3.9365E+05	4.0740E+05
23	0.2970	0.2350	--*	2.8064E+05	3.7384E+05	--*
28	0.2906	0.1977	0.2567	2.5566E+05	3.3885E+05	3.6659E+05

* --: missed measure test data

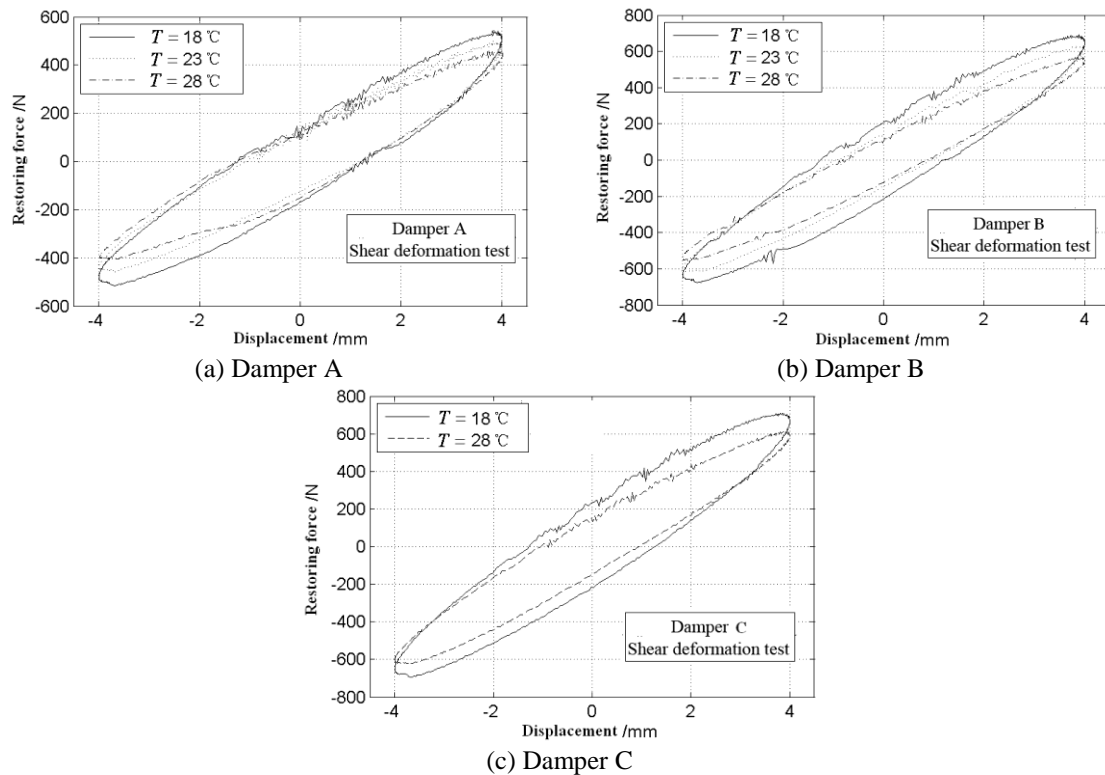


Fig. 11 Force-displacement curve of viscoelastic damper for different ambient temperatures

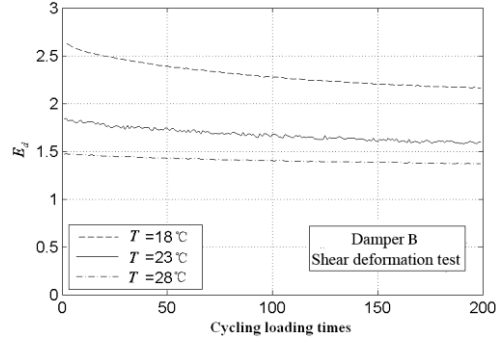


Fig. 12 The influence of cycling loading on the damper's absorption capacity

3.2.4 Influence of cycling loading times

In this section the strain amplitude is controlled by 40% and the excitation frequency is 1Hz. The relation curves of the circular dissipation per unit E_d and the loading times for the damper B at different ambient temperatures are shown in Fig. 12. It is noted from test results that the energy dissipation capacity of the VED will slightly decrease with the increase of loading times, and then will keep invariant after certain loading times.

3.3 Model establishment and numerical simulations

Three dimensional restoring forces of the VED are derived by the equivalent stiffness and equivalent damping model

$$p_{vex} = k'_x x + \frac{\eta_x k'_x}{\omega_x} \dot{x} \quad (2)$$

$$p_{vey} = k'_y y + \frac{\eta_y k'_y}{\omega_y} \dot{y} \quad (3)$$

$$p_{ve\theta} = k'_\theta \theta + \frac{\eta_\theta k'_\theta}{\omega_\theta} \dot{\theta} \quad (4)$$

where p_{vex} , p_{vey} and $p_{ve\theta}$ are the X-axis translational restoring force, Y-axis translational restoring force and Z-axis rotational restoring moment; $k'_x = G'_x A / \tau$, $k'_y = G'_y A / \tau$ and $k'_\theta = G'_\theta I_p / \tau$ denote the X-axis translational stiffness, Y-axis translational stiffness and Z-axis rotational stiffness, respectively; A and τ mean the shear area and thickness of viscoelastic material; $G'_i = G'(\omega_i)$, $i=x,y,\theta$ implies the storage modulus and $\eta_i = \eta(\omega_i)$, $i=x,y,\theta$ represents the loss factor. The expression of polar moment of inertia is $I_p = \beta h b^3$ for the rectangular shape of viscoelastic material layer and is $I_p = \pi d^4 / 32$ for the circular shape of viscoelastic material layer, where h and b are the length and width of viscoelastic material layer, and β is a coefficient related to the ratio of h to b and d is the diameter of viscoelastic material layer. In numerical simulation, G' and η are calculated by the improved equivalent standard solid model whose parameters are determined by the corresponding test data.

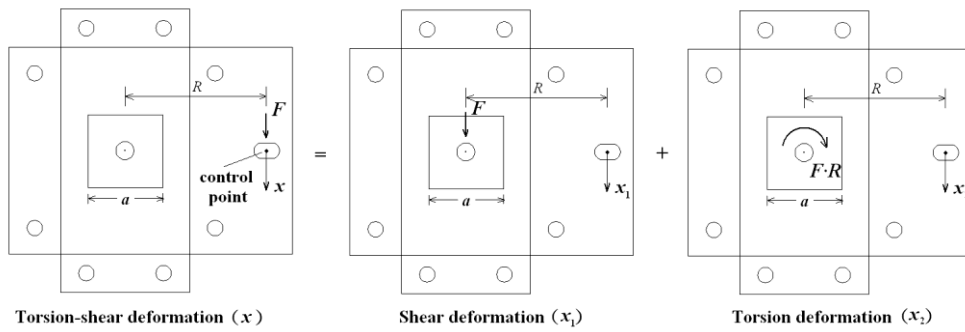


Fig. 13 Scheme of decomposition on torsion shear deformation

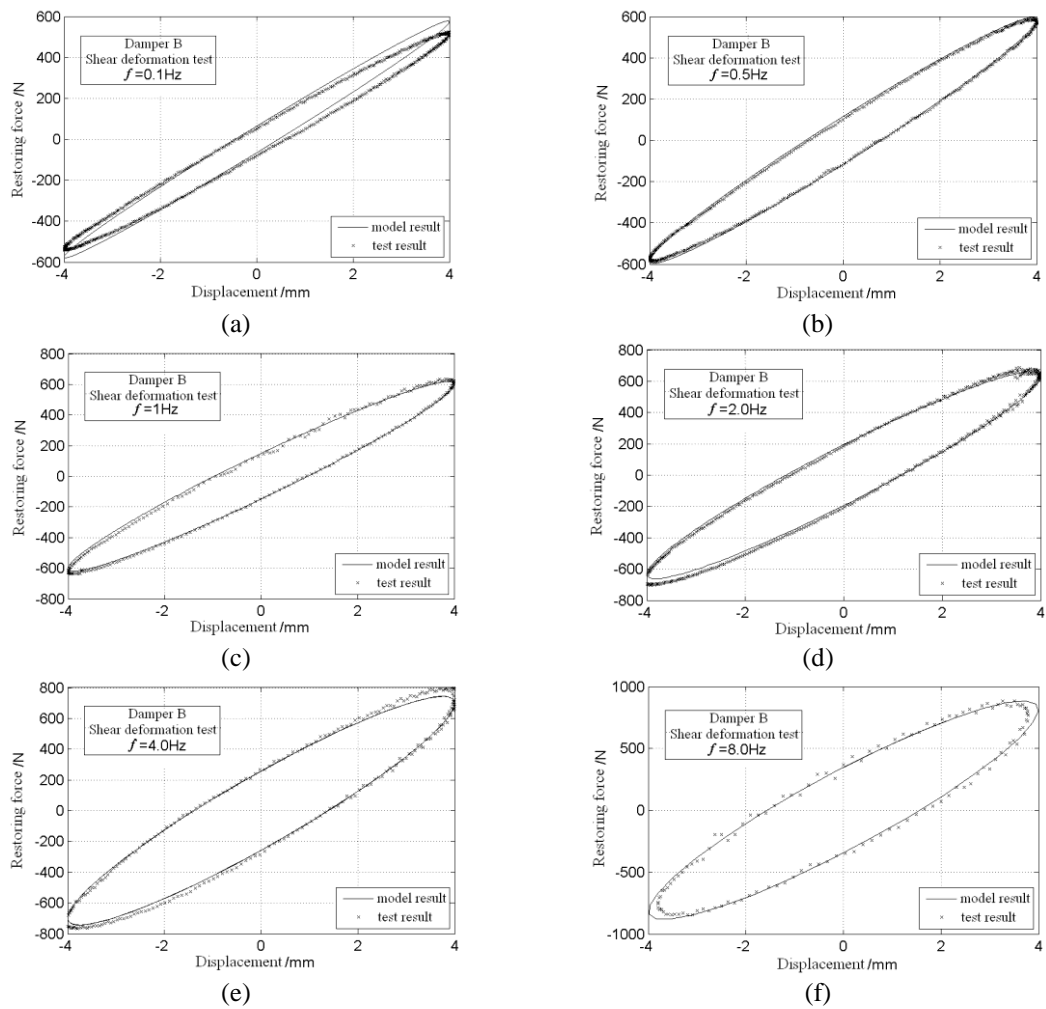


Fig. 14 Force-displacement curves of test results and model results (shear deformation test)

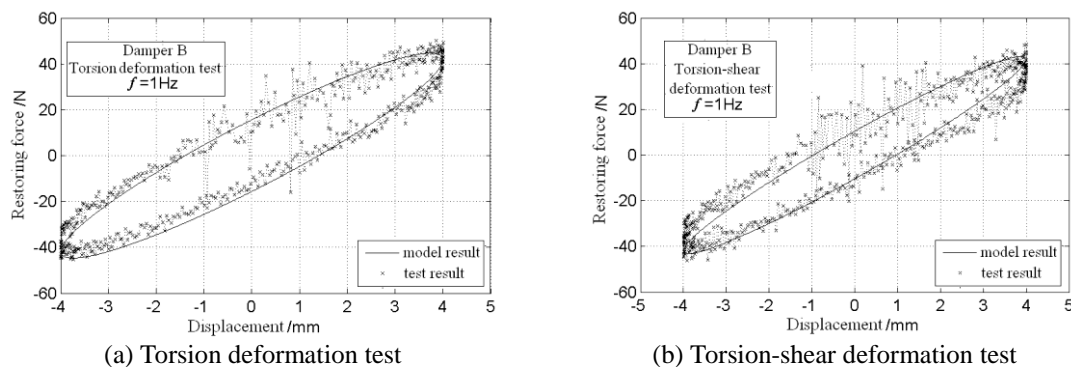


Fig. 15 Force-displacement curves of test results and model results(combined deformation test)

For shear and torsion deformation tests, the theoretic models of restoring force can be referred to Eqs. (2) and (4). For torsion-shear deformation tests, the theoretic model of restoring force is established based on the linear superposition principle without considering the coupling effect of deformations. Fig. 13 gives the force-displacement relationship between the control point and viscoelastic material. The comparisons of test results and numerical results on the restoring force curves with different excitation frequencies for shear deformation test are shown in Fig. 14. The test strain amplitude is controlled by 40% and ambient temperature is 23°C. The corresponding parameters for the improved equivalent standard solid model calculated by test data are $q_0=0.3586$, $q_1=0.1613$, $p_1=0.18062$, $c=1.19674$ and $d=0.37734$. For the torsion deformation and torsion-shear deformation tests, the comparisons of test and numerical results on the restoring force curves are shown in Fig. 15.

It can be concluded from the comparison results that the simulation precision of theoretical model of restoring force for the shear deformation are rather high for different excitation frequencies, and for torsion and torsion-shear deformations are both satisfied too. It is noted that the maximum restoring force is only about 50N for the torsion deformation test while it is over 600N for the shear deformation test when the maximum displacement of control point arrives at 4mm. It means that the equivalent stiffness and the circular dissipation per unit are much smaller for the torsion deformation than the shear deformation. This phenomena reveals that the energy dissipation capacity is very limited only by the single torsion deformation of the VED. In practical engineering application, the translational deformation of the VED should be fully used to dissipate much shaking energy.

4. Shaking table test on VED-damped frames

The control capacity of multi-dimensional seismic response for the new-type of the VED is rather absorbing for practical engineering. Due to its bi-directional deformation capacity, the VED can consume more energy than the normal VED. Here the shaking table test has been carried on a group of single-storey platform systems containing one symmetric platform and three asymmetric platforms with different eccentric forms in order to show their capacity of multi-dimensional response control.

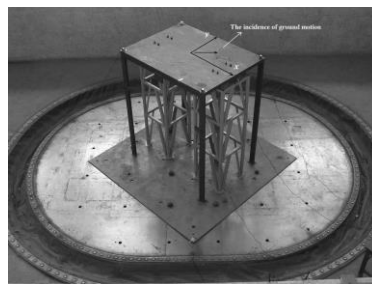
4.1 Test setup and program

4.1.1 Test purpose

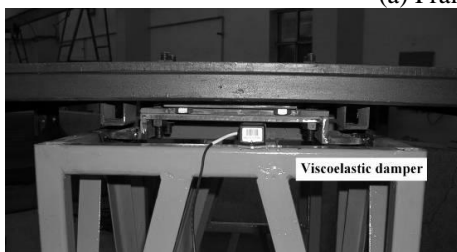
There are three purposes in this experiment: (1) to investigate the control capacity of multi-dimensional response of the VED for different platform systems including one symmetric platform and three asymmetric platforms with different eccentric forms; (2) to examine the control capacity of multi-dimensional response of the VED for different seismic wave incident angles including 0 degree (along X-axis), 45 degree and 90 degree (along Y-axis); (3) to study the control capacity of multi-dimensional response of the VED for different water conditions including waterless shaking table and underwater shaking table.

4.1.2 Test model and setup

The experiment is conducted on the shaking table of seismic laboratory of the DLUT (Dalian University of Technology). The basic test model is one-storey steel frame structure with the plan dimension of 1.2 m×0.9 m and the height of 1.4 m. Columns and beams for the frame are made from the box girder with dimension of 60 mm×30 mm×3 mm and diagonal braces are made by angle steel of 30 mm×30 mm×3 mm. The thickness of top plane is 10 mm. By changing the elements and masses, four platform systems may be made in the test, including: (1) the symmetric platform, (2) the mass eccentric platform, (3) the stiffness platform, (4) the mass-stiffness eccentric platform. The diagonal braces are only installed in one side for the stiffness eccentric platform and mass-stiffness eccentric platform, and are removed for the symmetric platform and mass eccentric platform. The additional lead block with the dimension of 150 mm×150 mm×60 mm is used for the mass eccentric platform and mass-stiffness eccentric platform. Three dimensional wireless acceleration transducers are used to measure the dynamic response of model. Fig. 16 gives the setup scheme of structure model and acceleration transducer. The distributing graph of the number and position for totally six transducers is shown in Fig. 17.



(a) Frame model with VED



(b) VED



(c) wireless three dimensional acceleration transducer

Fig. 16 Structure model and acceleration transducer

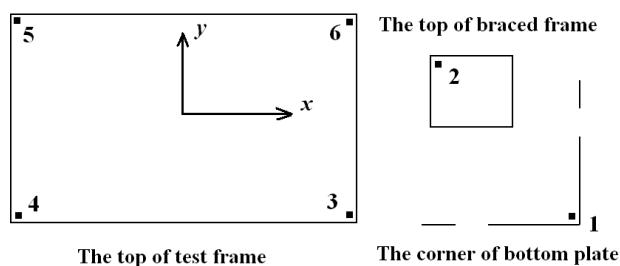


Fig. 17 Number and position for transducers

4.1.3 Test conditions

Totally five case conditions are conducted in the test. For every case, four earthquake acceleration records representing four kinds of ground soil sites are selected as inputs to the frame model. Unidirectional input of ground motion record along horizontal direction is considered in this test. Recorded earthquake ground motions of Tianjin (NS component, 1976 in China), El Centro (S00E component, 1940 in USA), Taft (S69E component, 1952 in USA) and Zhutang (S00E component, 1988 in China) with the peak value of acceleration adjusted to 0.2g are used in the experimental study. The test cases are as follows:

- (1) the incidence of seismic wave is 0 degree, and structure is uncontrolled in waterless shaking table;
- (2) the incidence of seismic wave is 45 degree, and structure is uncontrolled in waterless shaking table;
- (3) the incidence of seismic wave is 90 degree, and structure is uncontrolled in waterless shaking table;
- (4) the incidence of seismic wave is 90 degree, and structure is uncontrolled in underwater shaking table;
- (5) the structure is controlled with the new-type VED for the above all corresponding cases.

4.2 Results of test

The bi-directional frequency spectrums of the free and controlled structures under the white noise scanning (0.2 g) are shown in Fig. 18. It is seen from the figure that the fundamental frequencies along the two structure axes (X-axis and Y-axis) have been improved from 9.47 Hz and 5.57 Hz to 12.21 Hz and 7.91 Hz, respectively, after the VEDs are installed. Meanwhile the spectral peak values are reduced significantly. It means that the VED installed in the structure can absorb large amount of energy as well as increase the initial stiffness of the structure.

4.2.1 Results of different ground motions

Fig. 19 gives the bi-directional acceleration time-history curves of symmetric platform with 45 degree incidence for the four kinds of ground motions. Test results show that the VED designed here can effectively reduce the bi-axis vibrations for the structure simultaneously.

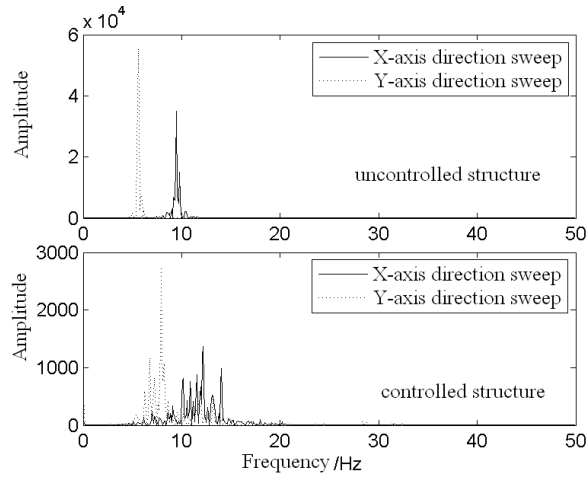
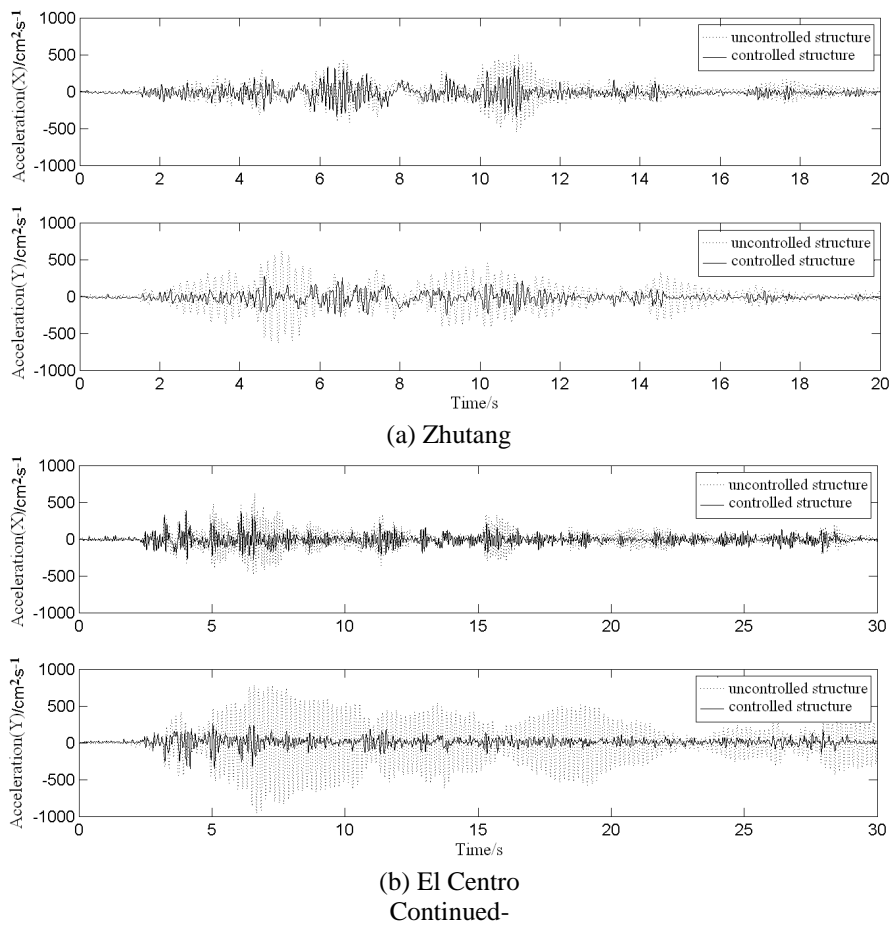


Fig. 18 Bi-directional frequency spectrums of the free and controlled structures



(b) El Centro
Continued-

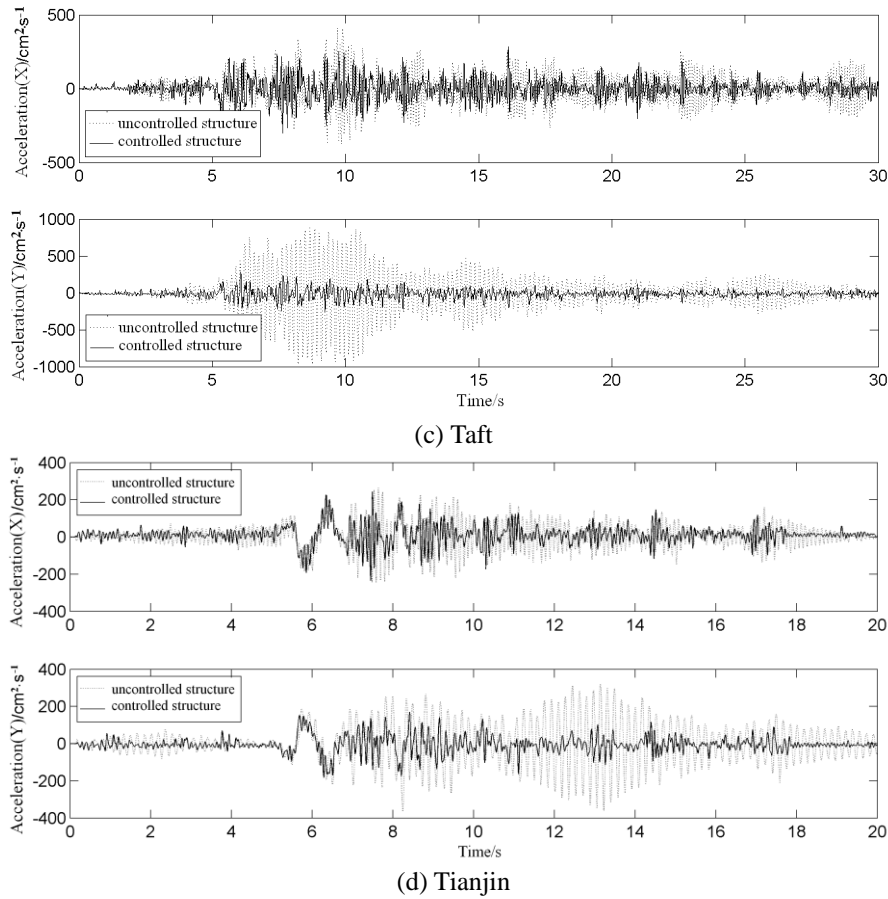


Fig. 19 Bi-directional acceleration time-history curves of symmetric platform with 45 degree incidence

Table 4 Acceleration control effect of asymmetric platform subjected to El Centro earthquake

	Node 6	0°incidence	45°incidence	90°incidence
X-axis direction	Uncontrolled structure/cm	694.2	535.9	105.9
	Controlled structure/cm	630.9	449.8	185.1
	Absorption ratio/%	9.12	16.07	-74.79
Y-axis direction	Uncontrolled structure/cm	417.1	741.5	692.9
	Controlled structure/cm	305.2	305.3	501.0
	Absorption ratio/%	26.83	58.83	27.70

4.2.2 Results of different seismic wave incidences

Table 4 gives the control effect of acceleration response of the node 6 for the mass-stiffness eccentric platform subjected to El Centro earthquake with different seismic wave incidences. Fig. 20 depicts the bi-directional displacement time-history curves of the node 5 for the same asymmetric platform with different seismic incidence. Test results show that the new-type VED can decrease the bi-axis vibrations for the asymmetric structure for different seismic incidence.

The control effect is more effective for the principle seismic direction, and it can reach about 60% for the displacement absorption ratio and get nearly 20% for the acceleration absorption ratio.

4.2.3 Results of different surrounding environments (underwater shaking and waterless shaking)

Tables 5 and 6 give the water-considered influence on the absorption ratio for the platform displacement and acceleration with 90 degree seismic wave incidence, respectively. Test results show that the control effect of the new-type VED on the dynamic response of platform structure for the underwater environment test will decrease slightly compared to the waterless environment test.

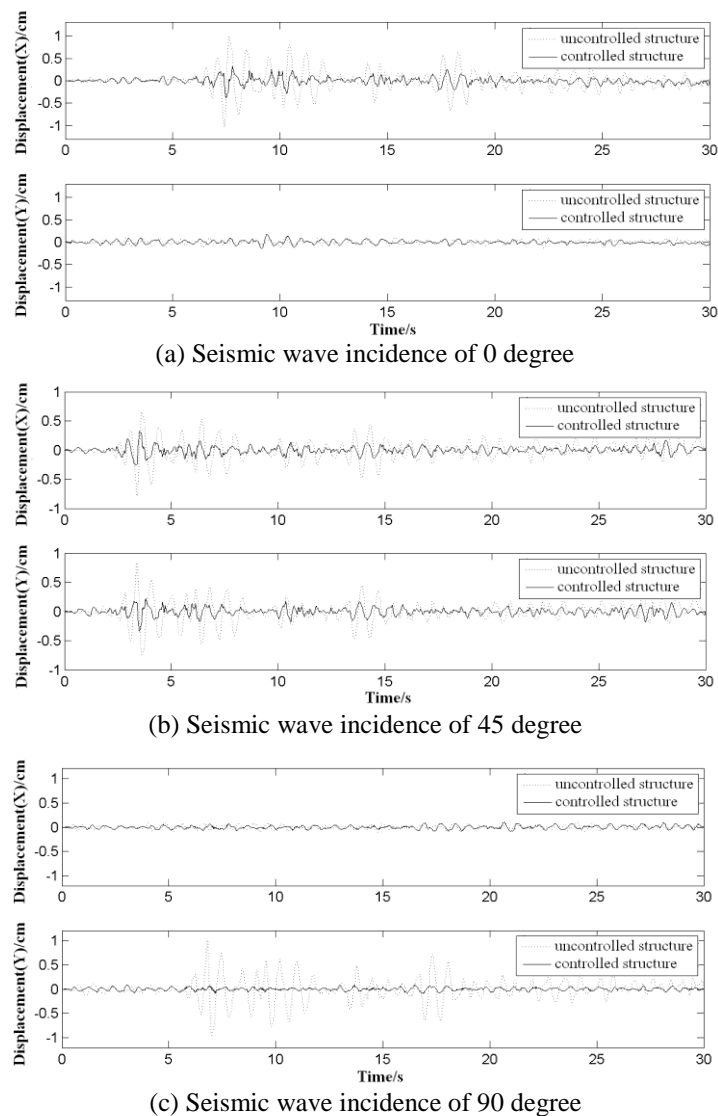


Fig. 20 Bi-directional displacement time-history curves of asymmetric platform with different incidence

4.3 Numerical simulations

Fig. 21 gives the comparisons of the displacement time histories between numerical calculations and experimental results for the symmetric platform subjected to El Centro earthquake with 45 degree wave incidence. Fig. 22 shows the corresponding comparisons of the X-direction acceleration time histories between numerical calculations and experimental results. It is seen from the comparison results that the numerical simulations is reliable and capable of reflecting the test results to a great extent. However, it is impossible that the two kinds of results are totally identical for inevitable error.

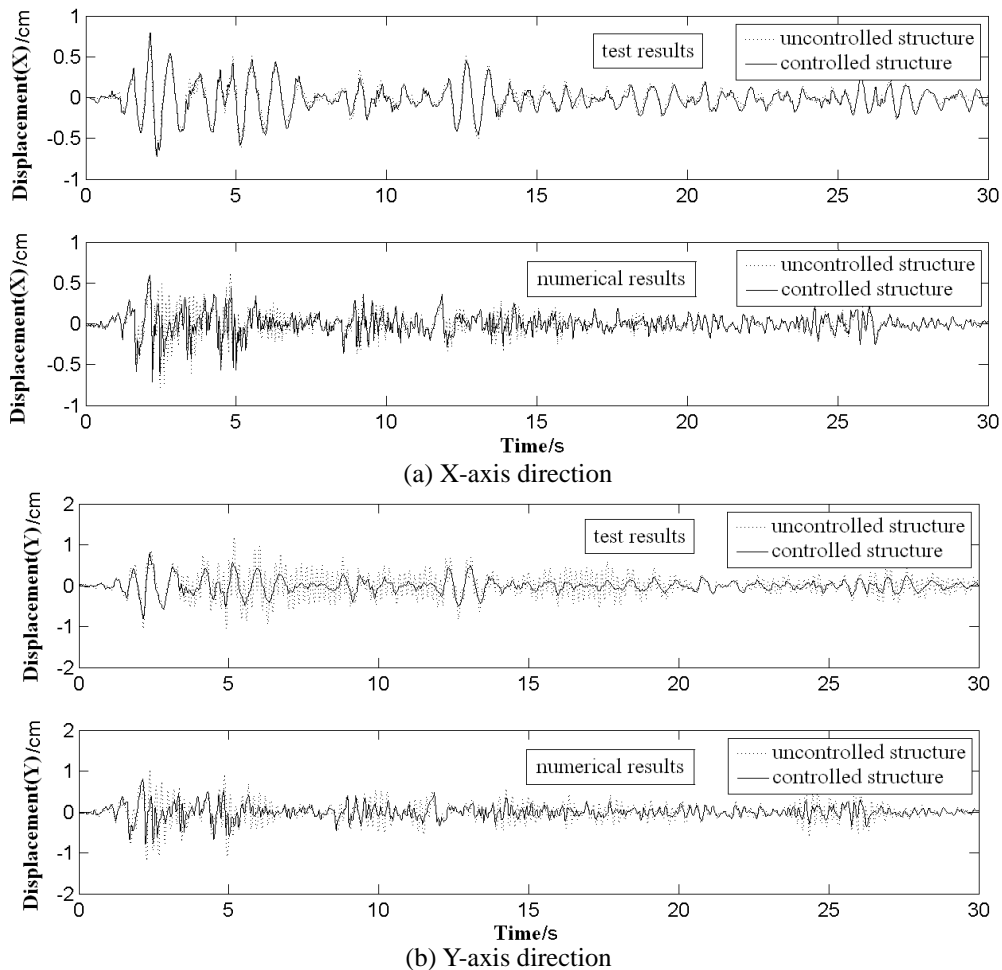


Fig. 21 Comparisons of displacement time histories between numerical calculations and experiments (El Centro, 45 degree)

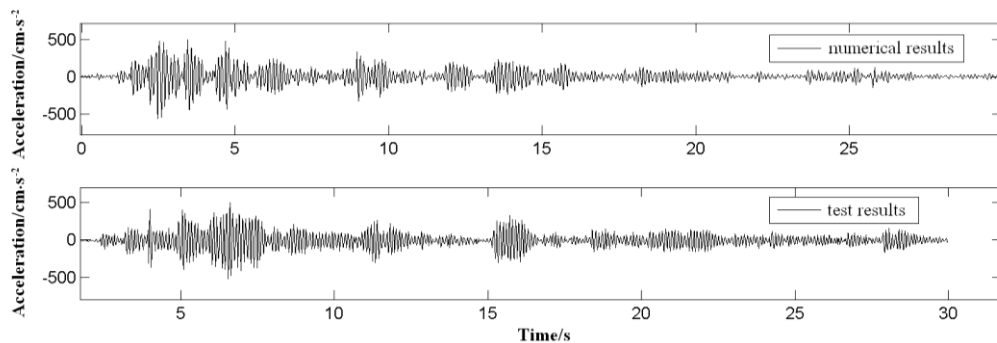


Fig. 22 Comparisons of X-direction acceleration time histories between numerical calculations and experiments (El Centro, 45 degree)

Table 5 Water-considered influence of on absorption ratio for platform displacement

maximum displacement /cm	Waterless environment			Underwater environment		
	Uncontrolled Structure	Controlled Structure	Absorption Ratio	Uncontrolled Structure	Controlled Structure	Absorption Ratio
Zhutang	0.9983	0.2175	78.21%	1.0269	0.5365	47.76%
El Centro	0.7565	0.2703	64.27%	1.1693	0.5123	56.19%
Taft	0.9618	0.2878	70.08%	0.8416	0.2773	67.05%
Tianjin	0.6363	0.3911	38.54%	0.6180	0.5711	7.59%

Table 6 Water-considered influence of water consideration on absorption ratio for platform acceleration

maximum acceleration /cm.s ⁻²	Waterless environment			Underwater environment		
	Uncontrolled Structure	Controlled Structure	Absorption Ratio	Uncontrolled Structure	Controlled Structure	Absorption Ratio
Zhutang	1026.4	494.0	51.87%	868.3	458.6	47.18%
El Centro	940.9	558.9	40.60%	873.5	561.1	35.76%
Taft	1145.8	455.4	60.25%	1091.8	462.9	57.60%
Tianjin	488.5	384.7	21.25%	447.1	382.5	14.45%

5. Conclusions

Experimental studies on the restoring force model of the new-type VED under various excited frequencies, strain amplitudes, ambient temperatures and cycling loading times have been carried out in this paper. Then, the control effect of multi-dimensional seismic response of the viscoelastic damper is also tested for various eccentric form structures subjected to different ground motions with different seismic wave incidences. The surrounding water environment is also considered here. The experimental results show that the simulation precision of the restoring force model is rather high for the shear deformation of viscoelastic damper and is also satisfied for the torsion deformation and the combined deformations with shear and torsion. The shaking table tests have verified that the new-type viscoelastic damper is effectively capable of mitigating the multi-dimensional seismic response of offshore platform. Suitable sizes of new-type VED can be designed according to the size of column-deck connection for the applied offshore platform project.

It can be installed on the every necessary column-deck joint, where the large deformation will produced. So the appearance design of offshore platform will not be influenced evidently.

Reference

- Bergman, D.M. and Hanson, R.D. (1993), "Viscoelastic mechanical damping devices tested at real earthquake displacements", *Earthq. Spectra*, **9**(3), 389-417.
- Bi, J. J. (1989), *Offshore Mechanics(in Chinese)*, Shanghai, Tongji University Press.
- Chang, K. C. and Soong, T.T. *et al.* (1995), "Seismic behavior of steel frame with added viscoelastic dampers", *J. Struct. Eng. - ASCE*, **121**(10), 1418-1426.
- Chang, K.C. and Soong, T.T. *et al.* (1992), "Ambient temperature on a viscoelastically damped structure", *J. Struct. Eng. - ASCE*, **118**(7), 1955-1973.
- Lee, H.H. (1997), "Stochastic analysis for offshore structures with added mechanical dampers", *Ocean Eng.*, **24**(9), 817-834.
- Lin, R.C. and Liang, Z. *et al.* (1991), "An experimental study on seismic behavior of viscoelastically damped structures", *Eng. Struct.*, **13**(1), 75-84.
- Ma, H.L. and Lu, J.H. *et al.* (2004), "Viscoelastic damper vibration control of platform with pole assignment technique(in Chinese)", *J. Ship Mech.*, **8**(4), 116-120.
- Mahmoodi, P. (1969), "Structural dampers", *J. Struct. Eng. Div. - ASCE*, **95**(10), 1661-1672.
- Ou, J.P. and Duan, Z.D. *et al.* (1999), "Ice-induced vibration analysis of JZ20-2MUQ offshore platform using in-situ ice force histories (in Chinese)", *Ocean Eng.*, **17**(2), 70-78.
- Ou, J.P. and Xiao, Y.Q. *et al.* (2000), "Ice-induced vibration control of JZ20-2MUQ Platform Structure with viscoelastic energy dissipators (in Chinese)", *Ocean Eng.*, **18**(3), 9-14.
- Ou, J.P. and Xu, L. *et al.* (2002), "Damping isolation system and its vibration-suppressed effectiveness analysis for offshore platform jacket structures (in Chinese)", *Earthq. Eng. Eng. Vib.*, **22**(3), 115-122.
- Zhou, Y. (2006), *Damping structural design by viscoelastic damper(in Chinese)*, Wuhan University of Technology Press, Wuhan, China.